Enhanced many-body effects in the excitation spectrum of a weakly interacting rotating Bose-Einstein condensate

Raphael Beinke,[1] Lorenz S. Cederbaum,[1] and Ofir E. Alon[2,3]

[1]*Theoretische Chemie, Physikalisch-Chemisches Institut, Universität Heidelberg, Im Neuenheimer Feld 229, D-69120 Heidelberg, Germany*

[2]*Department of Mathematics, University of Haifa, Haifa 3498838, Israel*

[3]*Haifa Research Center for Theoretical Physics and Astrophysics, University of Haifa, Haifa 3498838, Israel*

(Received 12 March 2018; published 30 November 2018)

The excitation spectrum of a highly condensed two-dimensional trapped Bose-Einstein condensate (BEC) is investigated within the rotating frame of reference. The rotation is used to transfer high-lying excited states to the low-energy spectrum of the BEC. We employ many-body linear-response theory and show that, once the rotation leads to a quantized vortex in the ground state, already the low-energy part of the excitation spectrum shows substantial many-body effects beyond the realm of mean-field theory. We demonstrate numerically that the many-body effects grow with the vorticity of the ground state, meaning that the rotation enhances them even for very weak repulsion. Furthermore, we explore the impact of the number of bosons N in the condensate on a low-lying single-particle excitation, which is describable within mean-field theory. Our analysis shows deviations between the many-body and mean-field results which clearly persist when N is increased up to the experimentally relevant regime, typically ranging from several thousand up to a million bosons in size. Implications are briefly discussed.

DOI: 10.1103/PhysRevA.98.053634

I. INTRODUCTION

Ultracold bosonic gases under rotation are suitable to probe various phenomena of correlated quantum systems. During the past two decades, rotating Bose-Einstein condensates (BECs) were studied from multiple perspectives, ranging from the occurrence of quantized vortices [1–5] to vortex lattices and excitations therein [6–8], and with respect to the analogy to the fractional quantum Hall effect [9–12]. The literature concerning these topics is extensive and we therefore refer to the reviews in Refs. [13–16].

In addition to analyzing the ground state of a rotating BEC, low-lying excited states have been of interest because for very low temperatures, they describe the thermodynamic properties of the system. Most studies offering analytical and numerical results for the low-energy spectra were carried out by utilizing the Bogoliubov–de Gennes (BdG) mean-field equation [17,18], e.g., the decay of the counter-rotating quadrupole mode [19], Tkachenko modes in vortex lattices [20,21], the twiston spectrum [22], or excitations in anharmonic traps [23,24]. Interestingly, a many-body analysis of the low-energy spectra in rotating BECs is rather rare. Examples are the yrast spectra in a harmonic confinement obtained by exact diagonalization [25–28].

The starting point and motivation of this work are different. We consider many-body effects in the low-energy excitation spectrum of a weakly interacting rotating BEC in a regime where the mean-field theory is supposed to accurately describe the physics. Going beyond previous works, we study bosons in an anharmonic external confinement [29–31] where one can no longer rely on the validity of the lowest Landau level approximation. The latter is well-suited for rapidly rotating and slightly repulsive bosons in a harmonic trap with rotation frequency very close to the trap frequency.

Rotating the BEC leads to a transfer of high-lying excited states in the laboratory frame to the low-energy part of the spectrum in the rotating frame. A central role in our analysis would be the dependence of the excitation energies and their many-body characteristics on the particle number N. It has been shown recently that for a nonrotating repulsive BEC in a trap, the excitation energies in the Hartree limit converge towards the BdG spectrum [32], and similarly for a rotating BEC under certain conditions [33]. However, it remains unclear if many-body effects in the excitation spectrum can be observed for mesoscopic and large BECs, typically of the experimentally relevant order of 10^3–10^6 bosons. Our numerical results present strong physical trends for this regime and show that the answer is positive.

As a main result, we show that once the rotation leads to a quantized vortex in the ground state, substantial many-body effects in the low-energy excitation spectrum occur. These effects grow with the vorticity of the ground state, which means they can be enhanced by stronger rotation. In addition, we demonstrate for a low-lying excited state which is also accessible within mean-field theory, that these effects clearly persist when the number of bosons is increased up to the experimentally relevant regime, despite the BEC being essentially condensed. The present work reports on accurate many-body excitation energies of a two-dimensional BEC obtained by linear response and goes well beyond previous investigations of one-dimensional systems [34,35].

II. SYSTEM AND METHODS

The general form of the Hamiltonian for N interacting bosons in the rotating frame is

given by

$$\hat{H}_{\rm rot} = \hat{H}_{\rm lab} - \Omega \hat{L}_z, \quad \hat{H}_{\rm lab} = \sum_{i=1}^{N} \hat{h}(\vec{r}_i) + \lambda_0 \sum_{i<j}^{N} \hat{W}(|\vec{r}_i - \vec{r}_j|), \tag{1}$$

where the single-particle Hamiltonian is $\hat{h} = -\frac{\Delta}{2} + V$ with the Laplacian $\Delta = \partial^2/\partial \vec{r}^{\,2}$ and the external trapping potential V, and the two-body interaction is $\lambda_0 \hat{W}$ with λ_0 being its strength. The rotation term contains the rotation frequency Ω and the total angular momentum operator in the z direction, $\hat{L}_z = \sum_{i=1}^{N} \hat{l}_z(i)$. We work in dimensionless units obtained by dividing $\hat{H}_{\rm rot}$ by $\frac{\hbar^2}{d^2 m}$ where d is a length scale and m the boson mass. A translation to dimensionful units is given in [36].

The Gaussian-shaped repulsion $\lambda_0 \hat{W}(|\vec{r}_i - \vec{r}_j|) = \frac{\lambda_0}{2\pi\sigma^2} e^{-|\vec{r}_i - \vec{r}_j|^2/2\sigma^2}$ with $\sigma = 0.25$ avoids the regularization problems of the zero-ranged contact potential in two dimensions [38,39], and has been employed in recent works [40–42,58,61,62]. The role of the width σ is discussed in Appendix A. The interaction strength λ_0 for different particle numbers is adjusted such that the mean-field interaction parameter $\Lambda = \lambda_0(N-1)$ is kept constant, i.e., $\lambda_0 \sim (N-1)^{-1}$. The trapping potential models a radially symmetric crater given by $V(r) = C\, e^{-0.5\,(r-R_C)^4}$ for $r = \sqrt{x^2+y^2} \leqslant R_C$ and $V(r) = C$ for $r > R_C$. The values of the crater height C and the radial size R_C are given in [36]. In contrast to the commonly considered harmonic trapping potential for rotating BECs, this potential ensures that the center-of-mass and relative coordinates do not separate. Furthermore, there is no formation of distinct Landau levels and it is thus required to go beyond the lowest Landau level approximation (see Appendix C).

The standard strategy to compute excited states in a (weakly interacting) BEC is to first calculate the ground state using the Gross-Pitaevskii (GP) equation [43–46]. In the rotating frame, it reads $[\hat{h} + \Lambda \int d\vec{r}\,' \hat{W}(|\vec{r} - \vec{r}\,'|)|\phi_{\rm GP}(\vec{r}\,')|^2 - \Omega \hat{l}_z]\phi_{\rm GP}(\vec{r}) = \mu\, \phi_{\rm GP}(\vec{r})$, where $\phi_{\rm GP}$ is the ground-state orbital and μ the chemical potential. Afterward, one applies linear-response theory atop $\phi_{\rm GP}$ which yields the BdG equation,

$$\mathcal{L}_{\rm BdG} \begin{pmatrix} u^k \\ v^k \end{pmatrix} = \omega_k \begin{pmatrix} u^k \\ v^k \end{pmatrix}, \tag{2}$$

with the BdG matrix $\mathcal{L}_{\rm BdG}$, the correction amplitudes u_k and v_k of the kth excited state to the ground-state orbital, and the excitation energies $\omega_k = E_k - E_0$ relative to the ground-state energy E_0. We employ the particle-conserving version of Eq. (2) [47–50]. It is worth noting that the BdG theory by construction only gives access to excitations where a single boson is excited from the condensed mode.

It is a well-known fact that a linear-response analysis atop the exact ground state gives rise to the exact excitation spectrum [51]. Thus, to go beyond the mean-field approach described above, we increase the accuracy of the ground state by utilizing a many-body ansatz for the wave function, $|\Psi(t)\rangle = \sum_{\vec{n}} C_{\vec{n}}(t)\,|\vec{n};t\rangle$, which is a superposition of permanents $\{|\vec{n};t\rangle\}$ comprised of M single-particle orbitals $\{\phi_j(\vec{r},t) : 1 \leqslant j \leqslant M\}$ and expansion coefficients $\{C_{\vec{n}}(t)\}$ where $\vec{n} = (n_1, \ldots, n_M)^t$ is a vector carrying the individual occupation numbers of the orbitals for a given permanent. Both the orbitals and coefficients are time adaptive and determined by the Dirac-Frenkel variational principle, yielding the multiconfigurational time-dependent Hartree for bosons (MCTDHB) method [52,53], see, e.g., [54–59] for applications.

The ground-state depletion f is defined as the occupation of all but the first natural orbital, $f = \sum_{k>1}^{M} n_k$. The natural orbitals are the eigenvectors of the one-body reduced density matrix $\boldsymbol{\rho} = \{\rho_{ij}\}$ with $\rho_{ij} = \langle \Psi | \hat{b}_i^\dagger \hat{b}_j | \Psi \rangle$ where the annihilation (creation) operator $\hat{b}_i^{(\dagger)}$ removes (adds) a particle from (to) the orbital ϕ_i. If only the largest occupation n_1 is macroscopic, the system is said to be condensed. This is the case in this work since the repulsion between the bosons is very weak. If more than a single occupation is macroscopic, the system is said to be fragmented, and there are recent works dealing with fragmented rotating BECs as well [42,60–62].

After computing the many-body ground state, we apply many-body linear-response (LR) theory, termed LR-MCTDHB [63,64], atop it, also see [34,35]. This leads to an eigenvalue equation of the form

$$\mathcal{L} \begin{pmatrix} \mathbf{u}^k \\ \mathbf{v}^k \\ \mathbf{C}_u^k \\ \mathbf{C}_v^k \end{pmatrix} = \omega_k \begin{pmatrix} \mathbf{u}^k \\ \mathbf{v}^k \\ \mathbf{C}_u^k \\ \mathbf{C}_v^k \end{pmatrix} \tag{3}$$

with the $(2M + N_{\rm conf})$-dimensional linear-response matrix $\mathcal{L}$ where $N_{\rm conf} = \binom{N+M-1}{N}$ is the number of possibilities to distribute N bosons among M orbitals. It consists of four blocks, $\mathcal{L} = \begin{pmatrix} \mathcal{L}_{oo} & \mathcal{L}_{oc} \\ \mathcal{L}_{co} & \mathcal{L}_{cc} \end{pmatrix}$, accounting for the couplings between the orbitals and coefficients. A detailed derivation of $\mathcal{L}$ and its submatrices is shown in [63,64]. The eigenvector $(\mathbf{u}^k, \mathbf{v}^k, \mathbf{C}_u^k, \mathbf{C}_v^k)^T$ collects the correction amplitudes to the ground-state orbitals and coefficients, and the eigenvalue $\omega_k = E_k - E_0$ denotes the energy of the kth excited state relative to the ground-state energy E_0. We stress that LR-MCTDHB also accounts for excitations where more than a single boson is excited from the condensed mode. It is further important to note that for $M = 1$, Eqs. (2) and (3) become identical such that the BdG theory is contained in our many-body approach as the simplest limiting case.

Throughout this work, we refer to excitations calculated with Eq. (2) as mean-field excitations, whereas to excitations calculated with Eq. (3) as many-body excitations. Furthermore, it is useful to distinguish between single- and multi-particle excitations where either one or multiple particles are excited from the condensed mode.

Technically, we calculate the lowest few eigenvalues of $\mathcal{L}$ by using the implicitly restarted Arnoldi method [65], a generalization of the Lanczos method for non-Hermitian matrices, and its parallel implementation in the ARPACK numerical library [66]. It allows us to treat even large systems with $N = 1000$ bosons and $M = 3$ orbitals, where already the dimensionality of the coefficient matrix $\mathcal{L}_{cc}$ exceeds 10^6. The numerical results below are converged both with respect to the number of orbitals M and the number of grid points on which

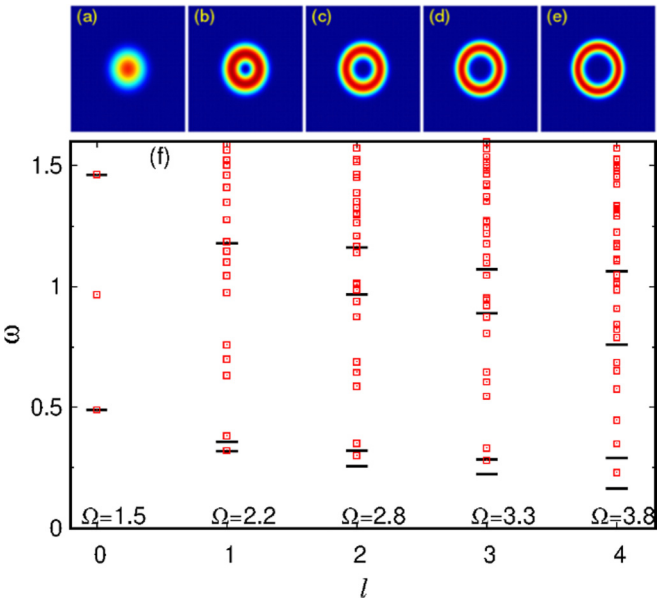

FIG. 1. (a)–(e) Many-body ground-state densities in a rotating BEC of $N = 10$ bosons with interaction parameter $\Lambda = 0.5$ for vorticities $l = 0$ to $l = 4$ [in respective panels (a)–(e)]. For $l > 0$ the ground state is a single vortex whose size grows with l. The mean-field densities are alike (not shown). (f) Corresponding low-energy excitation spectra for the ground states in the upper panels. Thick black lines indicate mean-field results from Eq. (2), i.e., with $M = 1$ (BdG), and red squares denote the many-body results from Eq. (3) with $M = 7$ orbitals (LR-MCTDHB). The many-body spectra show a very rich structure which cannot be accounted for within the mean-field picture. All quantities are dimensionless.

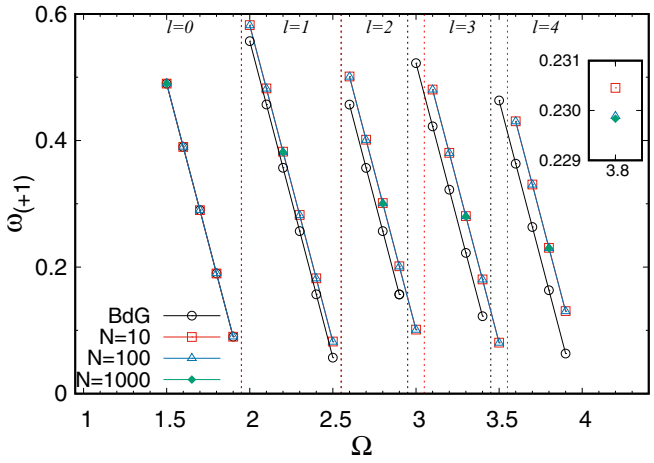

FIG. 2. Enhanced many-body effects by rotation. The excitation energies $\omega_{(+1)}$ are shown as a function of the rotation frequency Ω for interaction parameter $\Lambda = 0.5$. Many-body results are calculated for different particle numbers N. Vertical dotted lines indicate the transition from ground-state vorticity l to $l + 1$ between two adjacent analyzed rotation frequencies (mean-field in black and many-body in red). It is seen that the many-body effects grow with growing vorticity. Even the assignment of the vorticity to the mean-field and many-body ground states does not match as the vorticity grows, at least for systems up to $N = 1000$ bosons. The inset shows a magnified view for $\Omega = 3.8$. All quantities are dimensionless.

the Hamiltonian in Eq. (1) is represented. To calculate the ground states we use the MCTDHB implementation in [67].

III. RESULTS

Figure 1 shows the ground-state densities and the low-energy excitation spectra of a rotating BEC with $N = 10$ bosons and interaction parameter $\Lambda = 0.5$ for different rotation frequencies Ω. The many-body energies have been computed utilizing $M = 7$ orbitals which ensures numerical convergence for the shown energy range. A discussion on the numerical convergence can be found in Appendix A. The rotation frequencies were chosen such that the underlying ground states have different vorticities, i.e., angular momenta per particle, l. The degree of condensation $10 - f$ ranges from 9.999 ($l = 0$) to 9.962 ($l = 4$) out of 10 particles, meaning that the BEC is highly condensed and one might expect the mean-field theory to give accurate results. One can see from the densities in Figs. 1(a)–1(e) that the radial symmetry is, of course, preserved under rotation and that the core size of the vortex is growing with vorticity l. This is a giant vortex which an anharmonic trap can sustain [29,31], albeit here described at the many-body level.

With regard to the excitation spectra in Fig. 1(f), we observe that for $l = 0$, i.e., when the ground state is fully condensed, the mean-field and many-body energies of the first two single-particle excitations are equal (first and third state from below). They refer to the cases of taking one boson from the condensed mode to either an orbital with angular momentum $l_z = +1$ or $+2$, respectively. We refer to the former excitation as $(+1)$. How its energy $\omega_{(+1)}$ depends on the vorticity and the number of particles is discussed in detail below. The second excitation from below, only captured at the many-body level, is a two-particle excitation where two bosons occupy the orbital with $l_z = +1$.

For nonzero ground-state vorticities ($l > 0$), the deviations between the BdG and many-body spectra grow substantially. At the many-body level, the increased rotation transfers many more states to the low-energy spectrum than at the mean-field level. Moreover, the differences between BdG and many-body energies of single-particle excitations grow. The inaccuracy of the mean-field energies for single-particle excitations is intriguing since one might expect this simplest kind of excitations to be the least sensitive to many-body effects. In the remaining part of this work, we show that this intuition is misleading and that one needs an accurate many-body description even for the lowest single-particle excited states. Therefore, we elaborate on $(+1)$ in more detail.

Figure 2 shows the excitation energy $\omega_{(+1)}$ for a broader range of rotation frequencies Ω and compares mean-field and many-body energies for $N = 10$, 100, and 1000 bosons. Up to $\Omega = 1.9$ ($l = 0$), the mean-field and many-body results coincide, meaning that rotating the BEC with $\Omega \leqslant 1.9$ does not lead to visible many-body corrections to the excitation energy $\omega_{(+1)}$.

Once the ground state of the BEC becomes a vortex ($\Omega \geqslant 2.0$), the mean-field and many-body results start to deviate. The energetic distance between them grows with l. This can be rationalized by the geometry of a vortex. Since it has the

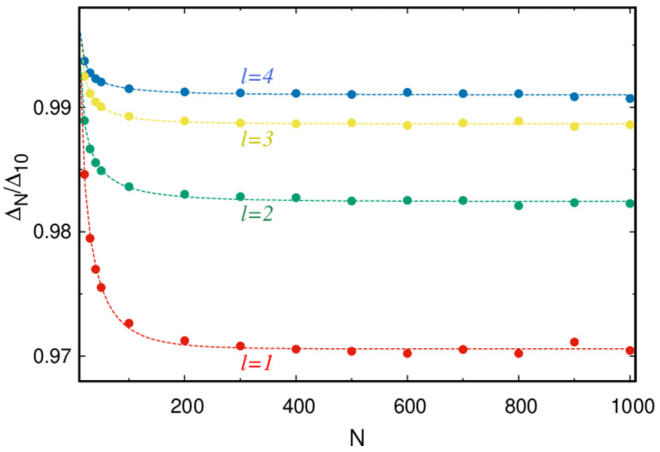

FIG. 3. Gap size Δ_N for particle numbers from $N = 20$ to $N = 1000$. Results are given relative to Δ_{10}, the dashed lines indicate exponential-fit curves. For $l = 0$, Δ_N is essentially zero (not shown). The gap varies with N weaker as the vorticity l grows. Small oscillations in the tails of the curves Δ_N/Δ_{10} are due to the numerical accuracy of order $O(10^{-5})$. All quantities are dimensionless.

shape of a ring with finite radial width, a comparison to a one-dimensional system of interacting bosons on a finite ring is instrumental. For such a system, it has been demonstrated recently that the overlap between the mean-field and the exact ground state decreases and that the depletion grows with the size of the ring [68]. This implies here that the quality of the BdG results decreases with growing vortex size and thus with growing vorticity. Nonetheless, we point out again that even for $N = 10$ and $l = 4$, f is only 0.038. Thus the BEC is highly condensed and one might *a priori* expect the BdG equation to yield accurate results for the lowest excitation energies. Instead, for $\Omega = 3.9$, the difference between the mean-field and many-body energies becomes approximately as large as the mean-field energy itself.

The inset in Fig. 2 magnifies $\omega_{(+1)}$ with respect to the particle number N for $\Omega = 3.8$. One can see that the excitation energy decreases as N grows, but increasing N from 100 to 1000 lowers $\omega_{(+1)}$ only marginally and one is rather far from the mean-field result.

Figure 3 shows the impact of N on the energy gap $\Delta_N = \omega^N_{(+1)} - \omega^{\mathrm{BdG}}_{(+1)}$, where $\omega^N_{(+1)}$ is the many-body and $\omega^{\mathrm{BdG}}_{(+1)}$ the mean-field energy of $(+1)$. Using $M = 3$ orbitals ensures numerical convergence for the obtained results of $\omega^N_{(+1)}$, see Appendix A. The gap size is shown relative to Δ_{10}, i.e., for $N = 10$ bosons. For all values of l, Δ_N decreases until $N \approx 200$ and then apparently slowly saturates. Moreover, the gap varies with N weaker as the vorticity l grows. Even for $l = 1$, the size of Δ_N remains around 97% of Δ_{10} for $N = 1000$, and it remains even larger for higher values of l. We stress again that the BEC is highly condensed for all chosen rotation frequencies. As an example, the degree of condensation for $N = 1000$ and $l = 4$ is 999.97, i.e., only $f \approx 0.03$ bosons (or 0.003%) are outside the condensed mode. According to the results in Fig. 3 there is basically no evidence that Δ_N would show a sharp descent when N is increased by two or three orders of magnitude beyond the particle numbers considered in this work. Naturally, the question arises whether the asymptotic behavior discussed in Refs. [32,33], namely, that the BdG spectrum yields the exact excitation energies for both trapped nonrotating and rotating but symmetry-broken BECs is the same for a rotating BEC where the radial symmetry is preserved. Although our results do not answer this question in general, they at least indicate that in such a case one would need an inconceivable amount of bosons to come close to the BdG energies, certainly more than 10^4–10^6 bosons which are typically used in experiments.

IV. CONCLUDING REMARKS

To summarize, we have shown that rotating a weakly interacting BEC leads to a strong enhancement of many-body effects in the low-energy excitation spectrum, even if the degree of condensation is very high. Besides the fact that the amount of multiparticle excited states increases strongly when the ground state is a vortex, the differences between the mean-field and accurate many-body excitation energies grow with growing vorticity and can become of the order of the mean-field excitation energies themselves, even for the very lowest single-particle excited states. Moreover, these differences clearly persist for larger particle numbers, showing that an accurate many-body theory for the low-energy excitation spectrum is necessary, not only for a small amount of bosons. Such many-body effects in the excitation spectrum would be interesting to search for also in the dynamics of essentially condensed rotating BECs.

ACKNOWLEDGMENTS

We thank Alexej I. Streltsov and Shachar Klaiman for many discussions. Computation time on the Cray XC40 cluster Hazel Hen at the High Performance Computing Center Stuttgart (HLRS) and the BwForCluster is acknowledged. R.B. acknowledges financial support by the IMPRS-QD (International Max Planck Research School for Quantum Dynamics), the Landesgraduiertenförderung Baden-Württemberg, and the Minerva Foundation. O.E.A. acknowledges funding by the Israel Science Foundation (Grant No. 600/15).

APPENDIX A: NUMERICAL CONVERGENCE

The numerical convergence of the results for the excitation energies shown in the main text is discussed. Furthermore, we discuss the convergence of the ground states themselves on top of which the linear-response analysis is applied, as well as the role of the width σ of the Gaussian interaction potential. A benchmark of the utilized numerical implementation of LR-MCTDHB [67] against the exactly solvable harmonic interaction model in two dimensions is shown in Appendix B.

Concerning the excitations, we focus on the convergence with respect to the number of orbitals M included in the LR-MCTDHB calculations and the number of grid points of the underlying spatial grid on which the orbitals are represented. For both cases, we show the convergence for a rotation frequency of $\Omega = 3.8$, i.e., $l = 4$, because for this vorticity the condensate depletion is maximal for the systems considered. The trap parameters are chosen as follows. For the radius of the crater we chose $R_c = 3.0$ and the height of the crater

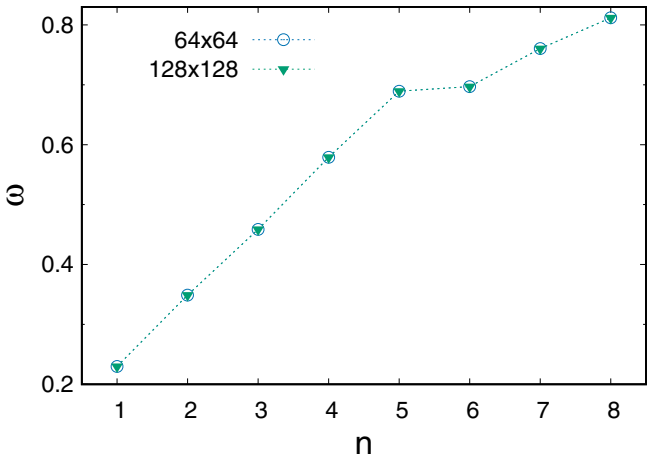

FIG. 4. Excitation energies of the lowest excited states for a BEC with $N = 100$ bosons, rotation frequency $\Omega = 3.8$ (i.e., ground-state vorticity $l = 4$), and interaction strength $\Lambda = 0.5$ for 64×64 and 128×128 grid points. Results are computed with LR-MCTDHB (3). The energies obtained for the two different grid sizes lie atop each other, showing numerical convergence for the smaller grid size. All quantities are dimensionless.

wall is $C = 200.0$, which is much larger than the energy per particle.

Figure 4 shows the lowest excitations for a BEC with $N = 100$ bosons, rotation frequency $\Omega = 3.8$, and interaction strength $\Lambda = 0.5$. We compare the results for a grid with 64×64 points to a grid with 128×128 points on a two-dimensional box with range $[-4, 4) \times [-4, 4)$. At the many-body level, $M = 3$ self-consistent orbitals are utilized within the MCTDHB approach. Comparing the results for the two different numbers of grid points, there are essentially no differences observable, the results lie atop each other. We observe a similar agreement also for other system parameters, i.e., different N, l, and Ω. We thus deduce that for all system

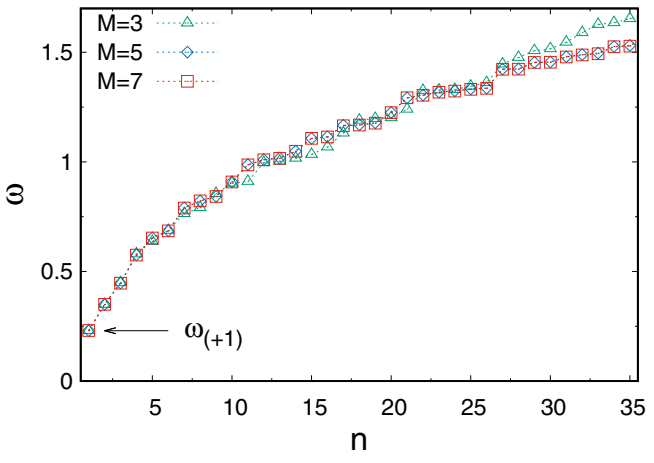

FIG. 5. Low-energy spectrum for system parameters $N = 10$, $\Omega = 3.8$, and $\Lambda = 0.5$. On the entire energy range, $M = 5$ orbitals yield accurate results. For the very lowest excitation energies, in particular for $\omega_{(+1)}$ which is discussed in detail in the main text, already $M = 3$ self-consistent orbitals lead to numerically converged values. All quantities are dimensionless.

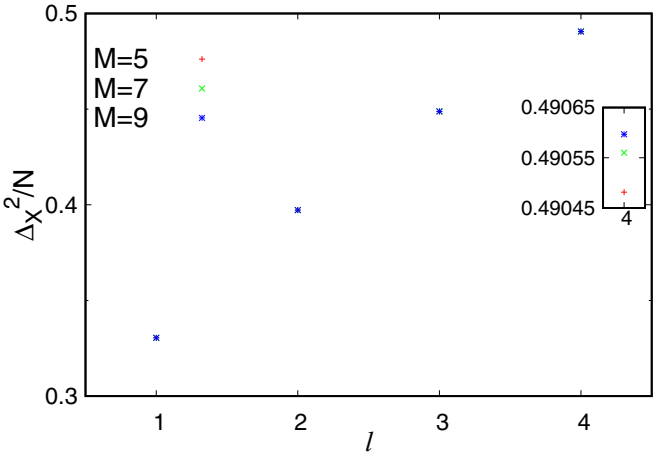

FIG. 6. Convergence of the position variance per particle in the x direction for the ground states of a BEC with $N = 10$ bosons and interaction strength $\Lambda = 0.5$ for different vorticities l. Results are computed for $M = 5$, 7, and 9 self-consistent orbitals. For all values of l, the points for different numbers of orbitals lie atop each other, demonstrating numerical convergence for $M = 5$. Inset: Magnified view for $l = 4$. Already for $M = 5$, the variance is converged to $O(10^{-3})$ of the exact value. All quantities are dimensionless.

parameters considered, the 64×64 grid yields converged results.

Figure 5 shows the comparison of the results for a BEC with parameters $N = 10$, $\Omega = 3.8$, and $\Lambda = 0.5$ for different numbers of orbitals M. There are two major observations. First, the results coincide for the very first excited states for all $M = 3$, 5, and 7. In particular, $M = 3$ orbitals lead to highly accurate results for the $(+1)$ excitation energy $\omega_{(+1)}$. Second, the results for $M = 5$ and 7 lie atop each other on the entire range shown, which is the same as in Fig. 1 of the main text. Thus, the results for $M = 5$ give an accurate description of the excitation energies up to $\omega = 1.5$. As for the discussion of the convergence with respect to the number of grid points, we observe a similar agreement also for other system parameters, i.e., different N, l, and Ω.

The numerical convergence of the ground-state energy and depletion is asserted during the computations of the results presented in the main text. Here we discuss the convergence of the position variance of the ground state in the x direction, i.e., the variance of the position operator $X = \sum_{i=1}^{N} x_i$, for the ground state of $N = 10$ bosons with interaction strength $\Lambda = 0.5$ and all values of $l > 0$ considered in the main text. It has been shown recently that the variance is a very sensitive quantity for many-body effects [69–73]. The position variance in the x direction of an N-boson system in two dimensions is given by

$$\frac{1}{N}\Delta_X^2 = \int d\mathbf{r}\,\frac{\rho(\mathbf{r})}{N}x^2 - \frac{1}{N}\left[\int d\mathbf{r}\,\rho(\mathbf{r})\,x\right]^2 + \int d\mathbf{r}_1 d\mathbf{r}_2\,\frac{\rho^{(2)}(\mathbf{r}_1,\mathbf{r}_2,\mathbf{r}_1,\mathbf{r}_2)}{N}x_1x_2, \quad \text{(A1)}$$

where $\mathbf{r} = (x, y)^t$, $\rho(\mathbf{r})$ denotes the one-body density at position $\mathbf{r}$, and $\rho^{(2)}$ denotes the two-body reduced density matrix. For further details on the derivation we refer to [69]. Figure 6

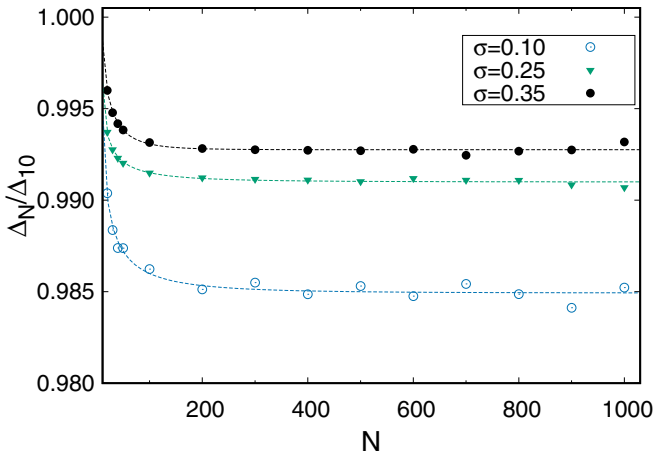

FIG. 7. Same as for the $l = 4$ vortex in Fig. 3 but for different widths σ of the Gaussian repulsion. As in the example of the main text ($\sigma = 0.25$), the relative gap Δ_N/Δ_{10} for the smaller and larger values of σ stays far away from zero, even for large BECs consisting of $N = 1000$ bosons. All quantities are dimensionless.

shows the many-body variance computed for different numbers of orbitals M. We observe that already utilizing $M = 5$ self-consistent orbitals yields numerical convergence since its results lie atop the results of $M = 7$ and $M = 9$. Only in a magnified view, differences of less than $O(10^{-3})$ can be seen (inset).

Finally, the role of the width σ of the Gaussian repulsion is discussed. Figure 7 shows the evolution of the gap Δ_N with respect to Δ_{10} [cf. Fig. 3] for the different widths. In all cases, the gap stays far away from zero, which would correspond to no many-body corrections to the BdG value of $\omega_{(+1)}$. One rather observes that for the smallest width of $\sigma = 0.1$, the gap remains to be approximately 98.5% of Δ_{10}, even for a large BEC with $N = 1000$ bosons, which is close to the values for $\sigma = 0.25$ from the main text. Hence the relative size and the persistence of the gap depend only slightly on the width of the Gaussian repulsion. This confirms that the physics is essentially governed by the weak depletion and the fact that high-lying excitations are transferred to the low-energy spectrum due to the rotation, and it does not depend on the details of the repulsive potential.

APPENDIX B: BENCHMARK TO THE HARMONIC INTERACTION MODEL

In this Appendix, we present a numerical benchmark of our newly developed implementation of LR-MCTDHB in two dimensions. As a reference, we chose the harmonic interaction model (HIM) in two spatial dimensions. As in the main text, results are shown for the rotating frame of reference.

In the HIM, both the trapping frequency and the two-body interaction potential are harmonic, i.e.,

$$V = \frac{1}{2}K^2\,\mathbf{r}^2 \tag{B1}$$

and

$$\hat{W}(\mathbf{r}_i, \mathbf{r}_j) = \lambda_0|\mathbf{r}_i - \mathbf{r}_j|^2, \tag{B2}$$

where positive (negative) λ_0 denotes attraction (repulsion) between the bosons. Below, we set $K = 1$ and $\lambda_0 = -0.001$. The rotation frequency is $\Omega = 0.1$. Table I shows the ground-state energy E_0 as well as the first 15 excitation energies $\omega_i = E_i - E_0$ for the mean-field case ($M = 1$) and the many-body case utilizing $M = 3$ self-consistent orbitals for $N = 100$ bosons. The exact results are obtained by applying the coordinate transformation

$$\mathbf{Q}_k = \frac{1}{\sqrt{k(k+1)}}\sum_{i=1}^{k}(\mathbf{r}_{k+1} - \mathbf{r}_i), \quad 1 \leqslant k \leqslant N-1, \tag{B3}$$

and

$$\mathbf{Q}_N = \frac{1}{\sqrt{N}}\sum_{i=1}^{k}\mathbf{r}_i, \tag{B4}$$

which separates the center-of-mass and relative motions of the bosons [74]. Also other coordinate transformations can be applied, see, e.g., Ref. [75]. The excitation energies for zero rotation are thus given by

$$E_{n,m} = \left(n + \frac{N-1}{2}\right)\tilde{\omega} + m + 1, \tag{B5}$$

with $\tilde{\omega} = \sqrt{K^2 \pm 2N\lambda_0}$. The parameters $n = 0, 2, 3, \ldots$ and $m = 0, 1, 2, \ldots$ denote the quantum numbers for excitations of the relative and center-of-mass coordinates, respectively. In the rotating frame, the above energy levels become shifted by the term

$$E_{\mathrm{rot}} = -\Omega\, l_z, \tag{B6}$$

where l_z denotes the angular momentum in the z direction. In Table I, we label all obtained excitations with the corresponding values (n, m, l_z). The numerical accuracy of the LR-MCTDHB (3) results becomes clearly obvious. The LR-MCTDHB many-body approach is superior to the BdG mean-field approach not only because it yields more accurate excitation energies, but also because all levels are obtained, so no state is missing for $M = 3$.

APPENDIX C: INAPPLICABILITY OF THE LOWEST LANDAU LEVEL APPROXIMATION

In this Appendix, we briefly discuss the inapplicability of the lowest Landau level approximation (LLL) for calculating the low-energy spectrum of excited states for the anharmonic trapping potential used in this work. The LLL, as described, e.g., in Ref. [16], is particularly appropriate to calculate the lowest excited states of rotating BECs in harmonic traps when the rotation frequency Ω is slightly lower than the trapping frequency K. In that case, all nodeless single-particle states with angular momenta $l_z = 0, 1, 2\ldots$ are energetically similar, and they are referred to as the lowest Landau level. The second lowest Landau level, referring to all states with one node, are energetically separated by $2K$. This separation of energies justifies the usage of the LLL, meaning that the wave function of the BEC can be approximated in terms of a full-configuration-interaction superposition where the underlying basis set is given by the first few states from the lowest Landau level. The LLL has been applied successfully

TABLE I. Spectra of excited states of the isotropic HIM in two dimensions in the rotating frame. The rotation frequency is $\Omega = 0.1$. Results are presented for $N = 100$ bosons and different numbers of orbitals M. The trapping frequency is $K = 1$, whereas the strength of the repulsive interaction is $\lambda_0 = -0.001$. Shown are the energies of the ground state E_0 and the first 15 excited states relative to E_0, $\omega_i = E_i - E_0$. Underlined figures show differences to the exact analytical results. All quantities are dimensionless.

	$M = 1$	$M = 3$	(n, m, l_z)	Exact analytical [Eqs. (B5)+(B6)]
E_0	89.554453	89.548293	(0,0,0)	89.548292
ω_1	0.900000	0.900000	(0,1,1)	0.900000
ω_2	1.100000	1.100000	(0,1,-1)	1.100000
ω_3	1.591089	1.588859	(2,0,2)	1.588854
ω_4	1.791089	1.788862	(2,0,0)	1.788854
ω_5		1.800439	(0,2,2)	1.800000
ω_6	1.991089	1.988859	(2,0,-2)	1.988854
ω_7		2.000657	(0,2,0)	2.000000
ω_8		2.200438	(0,2,-2)	2.200000
ω_9	2.386633	2.383226	(3,0,3)	2.383282
ω_{10}		2.487088	(2,1,3)	2.488854
ω_{11}	2.586634	2.583318	(3,0,1)	2.583282
ω_{12}		2.689270	(2,1,1)	2.688854
ω_{13}		2.691535	(2,1,1)	2.688854
ω_{14}		2.700528	(0,3,3)	2.700000
ω_{15}	2.786634	2.783318	(3,0,-1)	2.783282

in, e.g., Refs. [27,28]. We stress again that the separation from the second Landau level is crucial for the validity of the LLL.

To illustrate that the LLL is not applicable to the system considered in the main text, Fig. 8 shows several states of the first and second Lanau levels, computed with the BdG equation (2). The interaction strength is $\Lambda = 0.5$, as in the main text. The rotation frequency is $\Omega = 1.9$, which leads to a ground state with vorticity $l = 0$, but is very close to the transition to a vortex with vorticity $l = 1$. We are thus in a comparable situation to the case $\Omega \approx K$ in the harmonic trap. We see that the two Landau levels greatly overlap. Hence, there is no clear separation of the two levels, which shows that we are not in the regime where the LLL is applicable. Thus, one is in need of a more general approach like LR-MCTDHB to calculate the low-energy spectrum of the rotating BEC.

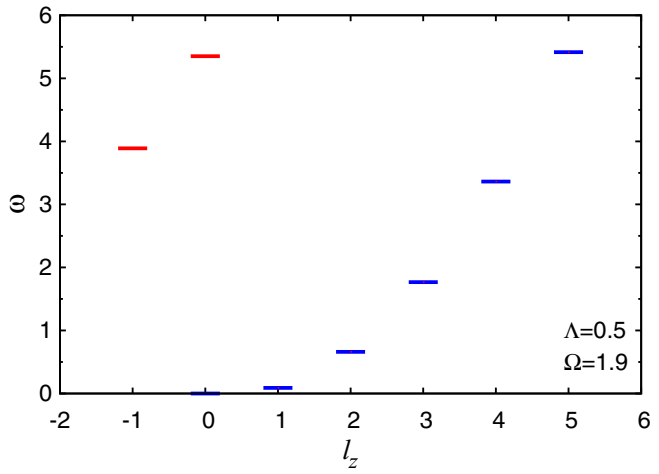

FIG. 8. Several states from the first two Landau levels in the case of the anharmonic trap utilized in this work, computed with the BdG equation. The angular momentum is denoted by l_z. Blue lines (for $l_z \geqslant 0$; to the right) denote the single-particle states (plus the ground state at $l_z = 0$) of the first level, red lines (for $l_z \leqslant 0$; to the left) denote the single-particle states of the second level. The rotation frequency $\Omega = 1.9$ is close to the transition of the ground state to a vortex with vorticity $l = 1$. The two Landau levels greatly overlap, showing that the LLL is not applicable here. All quantities are dimensionless.

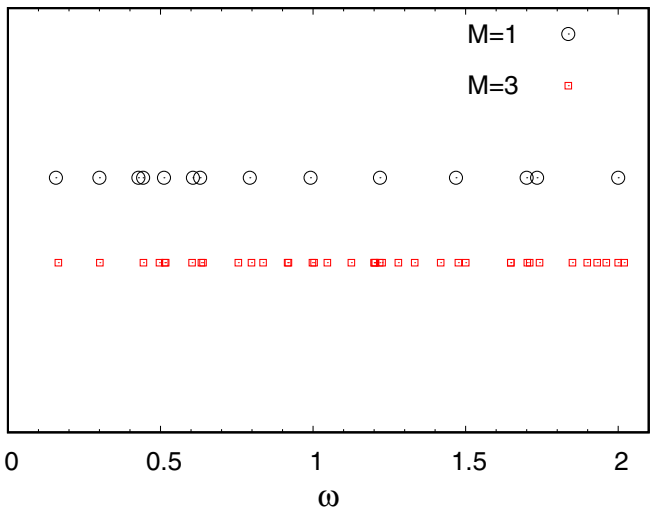

FIG. 9. Low-energy excitation spectrum for a rotating BEC in a harmonic trap. The number of bosons is $N = 100$ and the ground-state vorticity is $l = 1$. The repulsion is of the same Gaussian type as in the main text but with a width of $\sigma = 0.01$. The interaction parameter is $\Lambda = 0.5$. Compared are the results for the BdG spectrum ($M = 1$) and the many-body spectrum with $M = 3$ orbitals, leading to a depletion of $f \approx 1.65\%$. For $0 \leqslant \omega \lesssim 0.7$, the mean-field and many-body spectra deviate only slightly, whereas for higher excitation energies the differences become more pronounced. All quantities are dimensionless.

APPENDIX D: EXCITATIONS IN A HARMONIC TRAP

We qualitatively discuss many-body effects in the low-energy excitation spectrum of a rotating BEC in a harmonic trap, see Eq. (B1) with $K = 1$. To this end, we study excitations atop a vortex with vorticity $l = 1$ for a BEC consisting of $N = 100$ bosons, interacting via the same Gaussian repulsion as in the main text but with a smaller width of $\sigma = 0.01$. The interaction parameter is $\Lambda = 0.5$. In Fig. 9, the mean-field spectrum obtained from the BdG equation, i.e., Eq. (2), and the many-body spectrum obtained from LR-MCTDHB (3), i.e., Eq. (3), are compared. As for the anharmonic trap, we observe that the mean-field and many-body results show differences, both in terms of the number of states obtained as well as in the values of the excitation energies. This shows that many-body effects persist also in the harmonic trapping potential. However, although the depletion is higher ($f \sim 1.6\%$) than for the $l = 1$ vortex in the anharmonic trap of the main text ($f \sim 0.02\%$ for $N = 100$), the overall agreement between the mean-field and many-body spectra appears to be better, especially for the lowest excited states with energies $0 \leqslant \omega \lesssim 0.7$. This potentially means that the anharmonicity and the resulting coupling between the relative and center-of-mass motions enhances the occurrence of many-body effects. To investigate this further, also on a quantitative level, goes beyond the scope of this work and will be done elsewhere.

[1] D. A. Butts and D. S. Rokhsar, Nature (London) **397**, 327 (1999).
[2] M. R. Matthews, B. P. Anderson, P. C. Haljan, D. S. Hall, C. E. Wieman, and E. A. Cornell, Phys. Rev. Lett. **83**, 2498 (1999).
[3] K. W. Madison, F. Chevy, W. Wohlleben, and J. Dalibard, Phys. Rev. Lett. **84**, 806 (2000).
[4] F. Chevy, K. W. Madison, and J. Dalibard, Phys. Rev. Lett. **85**, 2223 (2000).
[5] K. W. Madison, F. Chevy, V. Bretin, and J. Dalibard, Phys. Rev. Lett. **86**, 4443 (2001).
[6] I. Coddington, P. Engels, V. Schweikhard, and E. A. Cornell, Phys. Rev. Lett. **91**, 100402 (2003).
[7] V. Schweikhard, I. Coddington, P. Engels, V. P. Mogendorff, and E. A. Cornell, Phys. Rev. Lett. **92**, 040404 (2004).
[8] A. Aftalion, X. Blanc, and J. Dalibard, Phys. Rev. A **71**, 023611 (2005).
[9] N. Regnault and T. Jolicoeur, Phys. Rev. Lett. **91**, 030402 (2003).
[10] S. Stock, B. Battelier, V. Bretin, Z. Hadzibabic, and J. Dalibard, Laser Phys. Lett. **2**, 275 (2005).
[11] C.-C. Chang, N. Regnault, T. Jolicoeur, and J. K. Jain, Phys. Rev. A **72**, 013611 (2005).
[12] M. Roncaglia, M. Rizzi, and J. Dalibard, Sci. Rep. **1**, 43 (2011).
[13] I. Bloch, J. Dalibard, and W. Zwerger, Rev. Mod. Phys. **80**, 885 (2008).
[14] N. R. Cooper, Adv. Phys. **57**, 539 (2008).
[15] S. Viefers, J. Phys.: Condens. Matter. **20**, 123202 (2008).
[16] A. L. Fetter, Rev. Mod. Phys. **81**, 647 (2009).
[17] N. N. Bogoliubov, J. Phys. (USSR) **11**, 23 (1947).
[18] P.-G. de Gennes, *Superconductivity of Metals and Alloys* (Benjamin, New York, 1966).
[19] T. Mizushima, M. Ichioka, and K. Machida, Phys. Rev. Lett. **90**, 180401 (2003).
[20] T. P. Simula and K. Machida, Phys. Rev. A **82**, 063627 (2010).
[21] L. O. Baksmaty, S. J. Woo, S. Choi, and N. P. Bigelow, Phys. Rev. Lett. **92**, 160405 (2004).
[22] F. Chevy, Phys. Rev. A **73**, 041604(R) (2006).
[23] A. Collin, Phys. Rev. A **73**, 013611 (2006).
[24] F. Ancilotto and F. Toigo, Phys. Rev. A **89**, 023617 (2014).
[25] S. Viefers, T. H. Hansson, and S. M. Reimann, Phys. Rev. A **62**, 053604 (2000).
[26] S. M. Reimann, M. Koskinen, Y. Yu, and M. Manninen, New J. Phys. **8**, 59 (2006).
[27] J. C. Cremon, G. M. Kavoulakis, B. R. Mottelson, and S. M. Reimann, Phys. Rev. A **87**, 053615 (2013).
[28] J. C. Cremon, A. D. Jackson, E. Ö. Karabulut, G. M. Kavoulakis, B. R. Mottelson, and S. M. Reimann, Phys. Rev. A **91**, 033623 (2015).
[29] U. R. Fischer and G. Baym, Phys. Rev. Lett. **90**, 140402 (2003).
[30] V. Bretin, S. Stock, Y. Seurin, and J. Dalibard, Phys. Rev. Lett. **92**, 050403 (2004).
[31] M. Correggi, F. Pinsker, N. Rougerie, and J. Yngvason, Eur. Phys. J. Spec. Top. **217**, 183 (2013).
[32] P. Grech and R. Seiringer, Commun. Math. Phys. **322**, 559 (2013).
[33] P. T. Nam and R. Seiringer, Arch. Rational Mech. Anal. **215**, 381 (2015).
[34] M. Theisen and A. I. Streltsov, Phys. Rev. A **94**, 053622 (2016).
[35] R. Beinke, S. Klaiman, L. S. Cederbaum, A. I. Streltsov, and O. E. Alon, Phys. Rev. A **95**, 063602 (2017).
[36] We use $R_C = 3.0$ and $C = 200.0$, meaning that C is higher than the energy per particle and the BEC is bound by the crater. Hence, the width of the Gaussian repulsion potential is clearly smaller than the trap crater, i.e., $\sigma < R_C$. To convert to real units, we suggest a condensate of ^{87}Rb atoms and a length scale of $d = 2\mu$m which yields 182.7 Hz as a unit of energy, such that the crater height is $C = 36.5$ kHz. With $R_C = 6\,\mu$m and an aspect ratio of $\frac{a_z}{R_C} = \frac{1}{200}$ between R_C and the transverse confinement a_z [42], the scattering length $a_s = \frac{\Lambda a_z}{(N-1)2\sqrt{2\pi}}$ [37] for $N = 10$ is given by $a_s = 0.67$ nm, and correspondingly lower values for higher boson numbers. By taking a weaker transversal confinement of $\frac{a_z}{R_C} = \frac{1}{20}$, the above values of a_s increase by a factor of 10.
[37] D. S. Petrov, M. Holzmann, and G. V. Shlyapnikov, Phys. Rev. Lett. **84**, 2551 (2000).
[38] C. N. Friedman, J. Funct. Anal. **10**, 346 (1972).
[39] R. A. Doganov, S. Klaiman, O. E. Alon, A. I. Streltsov, and L. S. Cederbaum, Phys. Rev. A **87**, 033631 (2013).
[40] J. Christensson, C. Forssén, S. Åberg, and S. M. Reimann, Phys. Rev. A **79**, 012707 (2009).
[41] S. Klaiman, A. U. J. Lode, A. I. Streltsov, L. S. Cederbaum, and O. E. Alon, Phys. Rev. A **90**, 043620 (2014).

[42] R. Beinke, S. Klaiman, L. S. Cederbaum, A. I. Streltsov, and O. E. Alon, Phys. Rev. A **92**, 043627 (2015).
[43] E. P. Gross, Nuovo Cimento **20**, 454 (1961).
[44] L. P. Pitaevskii, Zh. Eksp. Teor. Fiz. **40**, 646 (1961) [Sov. Phys. JETP **13**, 451 (1961)].
[45] L. P. Pitaevskii and S. Stringari, *Bose-Einstein Condensation* (Oxford University, Oxford, 2003).
[46] C. J. Pethick and H. Smith, *Bose-Einstein Condensation in Dilute Gases*, 2nd ed. (Cambridge University, New York, 2008).
[47] P. A. Ruprecht, M. Edwards, K. Burnett, and C. W. Clark, Phys. Rev. A **54**, 4178 (1996).
[48] Y. Castin and R. Dum, Phys. Rev. Lett. **79**, 3553 (1997).
[49] C. W. Gardiner, Phys. Rev A **56**, 1414 (1997).
[50] Y. Castin and R. Dum, Phys. Rev. A **57**, 3008 (1998).
[51] A. Fetter and J. D. Walecka, *Quantum Theory of Many-Particle Systems* (McGraw-Hill, New York, 1971).
[52] A. I. Streltsov, O. E. Alon, and L. S. Cederbaum, Phys. Rev. Lett. **99**, 030402 (2007).
[53] O. E. Alon, A. I. Streltsov, and L. S. Cederbaum, Phys. Rev. A **77**, 033613 (2008).
[54] K. Sakmann, A. I. Streltsov, O. E. Alon, and L. S. Cederbaum, Phys. Rev. Lett. **103**, 220601 (2009).
[55] J. Grond, T. Betz, U. Hohenester, N. J. Mauser, J. Schmiedmayer, and T. Schumm, New J. Phys. **13**, 065026 (2011).
[56] I. Brouzos, A. I. Streltsov, A. Negretti, R. S. Said, T. Caneva, S. Montangero, and T. Calarco, Phys. Rev. A **92**, 062110 (2015).
[57] S. I. Mistakidis, L. Cao, and P. Schmelcher, Phys. Rev. A **91**, 033611 (2015).
[58] U. R. Fischer, A. U. J. Lode, and B. Chatterjee, Phys. Rev. A **91**, 063621 (2015).
[59] V. J. Bolsinger, S. Krönke, and P. Schmelcher, Phys. Rev. A **96**, 013618 (2017).
[60] D. Dagnino, N. Barberán, M. Lewenstein, and J. Dalibard, Nat. Phys. **5**, 431 (2009).
[61] K. Sakmann and M. Kasevich, Nat. Phys. **12**, 451 (2016).
[62] S. E. Weiner, M. C. Tsatsos, L. S. Cederbaum, and A. U. J. Lode, Sci. Rep. **7**, 40122 (2017).
[63] J. Grond, A. I. Streltsov, A. U. J. Lode, K. Sakmann, L. S. Cederbaum, and O. E. Alon, Phys. Rev. A **88**, 023606 (2013).
[64] O. E. Alon, A. I. Streltsov, and L. S. Cederbaum, J. Chem. Phys **140**, 034108 (2014).
[65] Y. Saad, *Numerical Methods for Large Eigenvalue Problems* (Halstead, New York, 1992).
[66] http://www.caam.rice.edu/software/ARPACK/
[67] A. I. Streltsov, L. S. Cederbaum, O. E. Alon, K. Sakmann, A. U. J. Lode, J. Grond, O. I. Streltsova, S. Klaiman, and R. Beinke, The Multiconfigurational Time-Dependent Hartree for Bosons Package, version 3.x, http://mctdhb.org, Heidelberg/Kassel (2006-present).
[68] L. S. Cederbaum, Phys. Rev. A **96**, 013615 (2017).
[69] S. Klaiman and O. E. Alon, Phys. Rev. A **91**, 063613 (2015).
[70] S. Klaiman, A. I. Streltsov, and O. E. Alon, Phys. Rev. A **93**, 023605 (2016).
[71] S. Klaiman, A. I. Streltsov, and O. E. Alon, J. Phys.: Conf. Ser. **826**, 012020 (2017).
[72] S. Klaiman, R. Beinke, L. S. Cederbaum, A. I. Streltsov, and O. E. Alon, Chem. Phys. **509**, 45 (2018).
[73] S. K. Haldar and O. E. Alon, Chem. Phys. **509**, 72 (2018).
[74] L. Cohen and C. Lee, J. Math. Phys. **26**, 3105 (1985).
[75] J. Yan, J. Stat. Phys. **113**, 623 (2003).